Aspects of Gravitational Clustering

Jayanti Prasad

National Centre for Radio Astronomy
Pune, India (411007)

September 23, 2009

Plan of the Talk

- Nonlinear Gravitational Clustering
- Role of substructure
- Finite Volume Effects In N-body Simulations
- Summary & Conclusions

Introduction

Matter distribution in the Universe

Large scale (earlier time)	Small scales (recent time)
Smooth	Clumpy

Question: How structures in the Universe formed ?
Answer : Gravitational Instability

Basic Equations

- **Density Contrast:**

$$\begin{aligned} \delta(\mathbf{x},t) &= \frac{\rho(\mathbf{x},t)-\rho_b(t)}{\rho_b(t)} \\ \delta_{\mathbf{k}}(t) &= \int \frac{d^3x}{V}\delta(\mathbf{x},t)\exp(-i\mathbf{k}.\mathbf{x}) \end{aligned} \tag{1}$$

- **Equation of motion:**

$$\begin{aligned} \ddot{\mathbf{x}}_i + 2\frac{\dot{a}}{a}\dot{\mathbf{x}}_i &= -\frac{1}{a^2}\nabla_i\varphi \\ \nabla^2\varphi = 4\pi G a^2(\rho-\bar{\rho}) &= \frac{3}{2}\frac{\delta}{a^3}H_0^2\Omega_{nr} \\ \rho(\mathbf{x}) &= \frac{1}{a^3}\sum_i m_i\delta_D(\mathbf{x}-\mathbf{x}_i) \end{aligned} \tag{2}$$

- **Mode coupling:**

$$\ddot{\delta}_{\mathbf{k}} + 2\frac{\dot{a}}{a}\dot{\delta}_{\mathbf{k}} = \frac{3}{2}\frac{\delta_{\mathbf{k}}}{a^3}H_0^2 + A_k - B_k \tag{3}$$

where

$$A_k = \frac{3}{4}\frac{1}{a^3}H_0^2 \sum_{\mathbf{k}'\neq 0,\mathbf{k}} \left[\frac{\mathbf{k}.\mathbf{k}'}{k'^2} + \frac{\mathbf{k}.(\mathbf{k}-\mathbf{k}')}{|\mathbf{k}-\mathbf{k}'|^2}\right] \delta_{\mathbf{k}'}\delta_{\mathbf{k}-\mathbf{k}'}$$

and

$$B_k = \frac{1}{M}\sum_i m_i \left(\mathbf{k}.\dot{\mathbf{x}}_i\right)^2 \exp\left[i\mathbf{k}.\mathbf{x}_i\right] \quad ; \quad M = \sum_i m_i$$

Two problems addressed in the thesis

- *Structure formation in a cold dark matter dominated universe takes place hierarchically. In this situation it becomes relevant to ask:*
  what role perturbations at small scales (substructure) play in the collapse of perturbations at larger scales ?.
  –Transverse motions can help in relaxation.
- *It is well knows that there are strong effects of perturbations at large scales on the growth of perturbations at small scales. In cosmological N-body simulations perturbations at scales larger than the size of simulation volume are ignored:*
  How the size of simulation volume affect various physical quantities in N-body simulations ?
  –Can modify clustering properties.

STUDY 1

A. Gravitational collapse in an expanding background and the role of substructure

References:

- Bagla, J. S., **Prasad, Jayanti** and Ray, Suryadeep, 2005, MNRAS, 360, 194, (astro-ph/0408429) *Gravitational collapse in an expanding background and the role of substructure I: Planar collapse*
- Bagla, J. S., **Prasad, Jayanti** 2008, MNRAS, 1365, 2966 (arXiv:0802.2796 [astro-ph]), *Gravitational collapse in an expanding background and the role of substructure II: Excess power at small scales and its effect of collapse of structures at larger scales.*

Planar Collapse

Table 1. This table lists the parameters of N-body simulations we have used. All the simulations used 128^3 particles. The first column lists the name of the simulation, the second column lists the code that was used for running the simulation, the third column gives the relative amplitude of small-scale power and the plane wave, the fourth column tells us whether the large-scale plane wave was present in the simulation or not, and the last column lists the distribution of particles before these are displaced using a realization of the power spectrum. *Grid* distribution means that particles started from grid points. *Perturbed grid* refers to a distribution where particles are randomly displaced from the grid points; this displacement has a maximum amplitude of 0.05 grid points. Such an initial condition is needed to prevent particles from reaching the same position in plane-wave collapse as such a situation is pathological for tree codes. The TREEPM simulations were run with a force softening length equal to the grid length.

Name	Method	α	Plane wave	IC
PM_00L	PM	0.0	Yes	Grid
T_00L	TREEPM	0.0	Yes	Perturbed grid
T_05L	TREEPM	0.5	Yes	Grid
T_10L	TREEPM	1.0	Yes	Grid
T_20L	TREEPM	2.0	Yes	Grid
T_40L	TREEPM	4.0	Yes	Grid
T_10P	TREEPM	1.0	Yes	Perturbed grid
T_40P	TREEPM	4.0	Yes	Perturbed grid
T_05	TREEPM	0.5	No	Grid
T_10	TREEPM	1.0	No	Grid
T_20	TREEPM	2.0	No	Grid
T_40	TREEPM	4.0	No	Grid

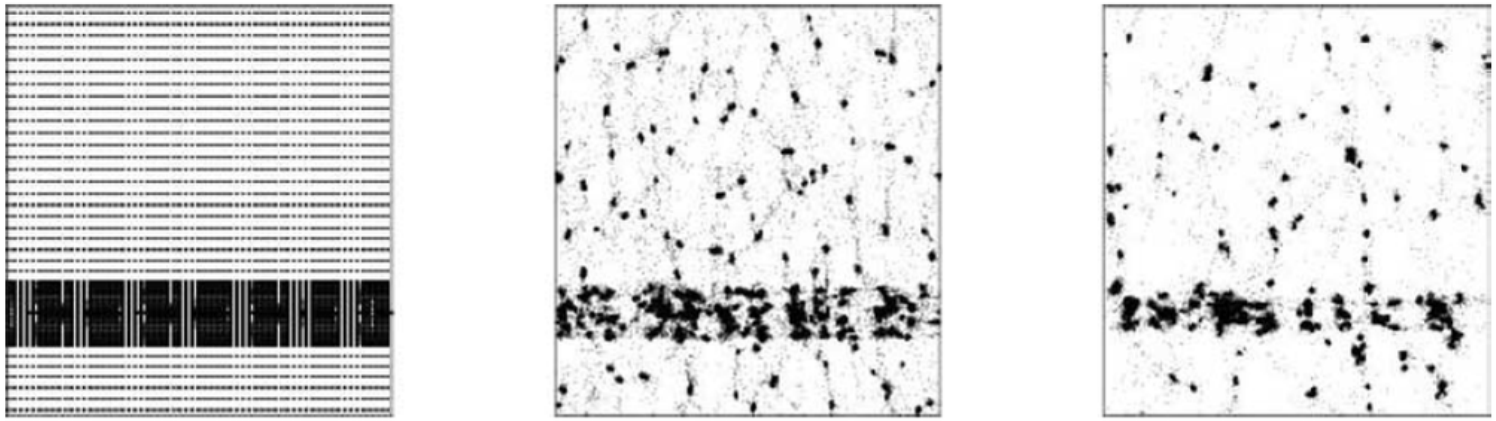

Figure 3. Panels in this figure show the same slice from simulation T_00L, T_10L and T_40L. These slices are shown for $a = 2$, the plane wave begins to collapse at $a = 1$. The plane wave collapses along the vertical direction in these slices. The left panel is for T_00L, the middle panel is for T_10L and the right panel is for T_40L.

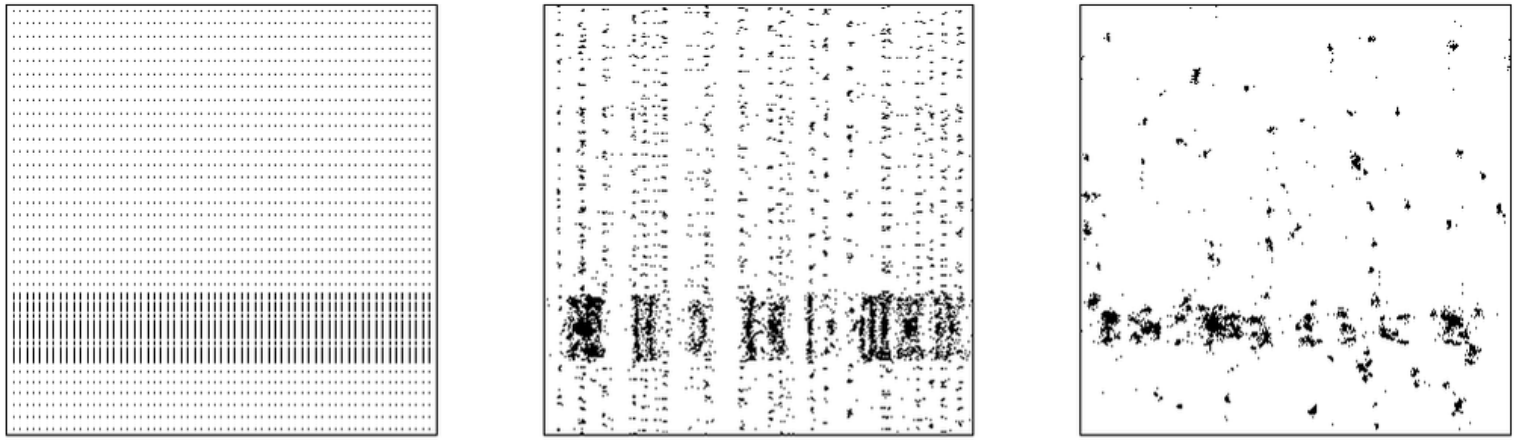

Figure 5. This figure shows slices from simulations T_40L and T_40P for $a = 2$. The left panels shows a slice from the simulation PM_00L, plotted here for reference. The central panel is for T_40P and the right panel is for T_40L. This visual comparison shows that the pancake is thinner in T_40L as compared to T_40P. Indeed, the thickness of the pancake in T_40P and PM_00L is very similar.

© 2005 RAS, MNRAS **360**, 194–202

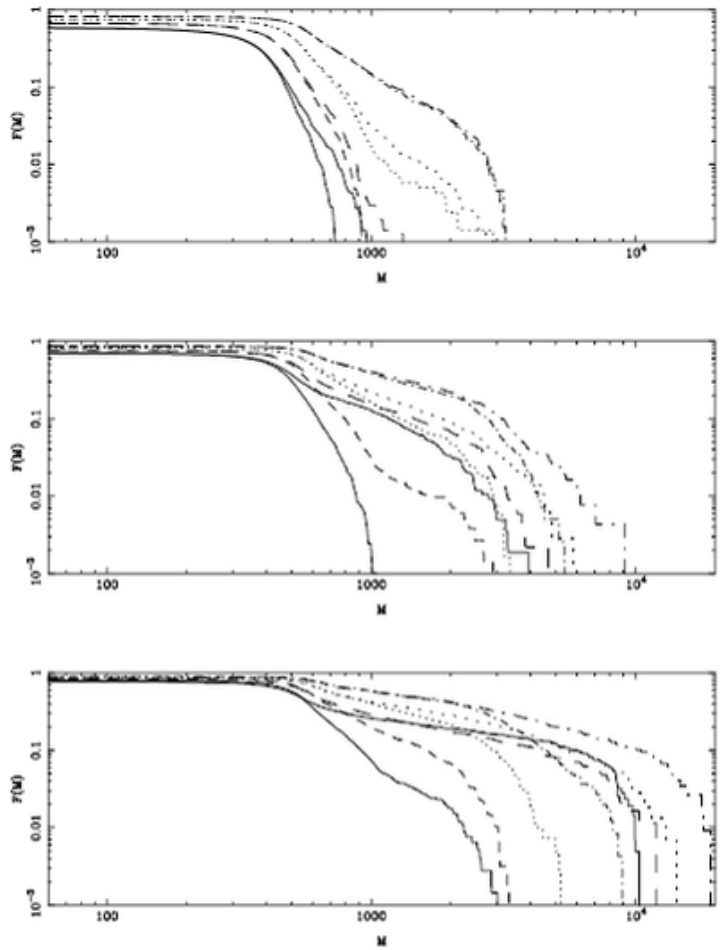

Figure 9. This figure shows the cumulative mass function $F(M)$ as a function of mass M in N-body simulations. The top panel is for $a = 0.5$, the middle panel is for $a = 1$ and the lower panel is for $a = 2$. Curves are shown for T_05 (solid curve), T_05L (thick solid curve), T_10 (dashed curve), T_10L (thick dashed curve), T_20 (dotted curve), T_20L (thick dotted curve), T_40 (dot-dashed curve) and T_40L (thick dot-dashed curve).

B. Features in $P(k)$

- Models:

$$P(k) = \begin{cases} Ak^{-1}, & \text{for Model I} \\ Ak^{-1} e^{-\frac{k^2}{2k_c^2}}, & \text{for Model II} \\ Ak^{-1} + A\alpha k_c^{-1} e^{\frac{(k-k_c)}{2\sigma_k^2}} & \text{for Model III} \end{cases} \quad (4)$$

- Parameters:
  $\sigma_k = 2\pi/L_{box}$, $k_c = 4k_f = 4(2\pi/L_{bpx})$, $\alpha = 4$
  $r_{nl}(a = 1) = 12$, $N_{part} = 200^3$, $L_{box} = 200$
- Code: TreePM(Bagla 2002, Bagla & Ray 2003).

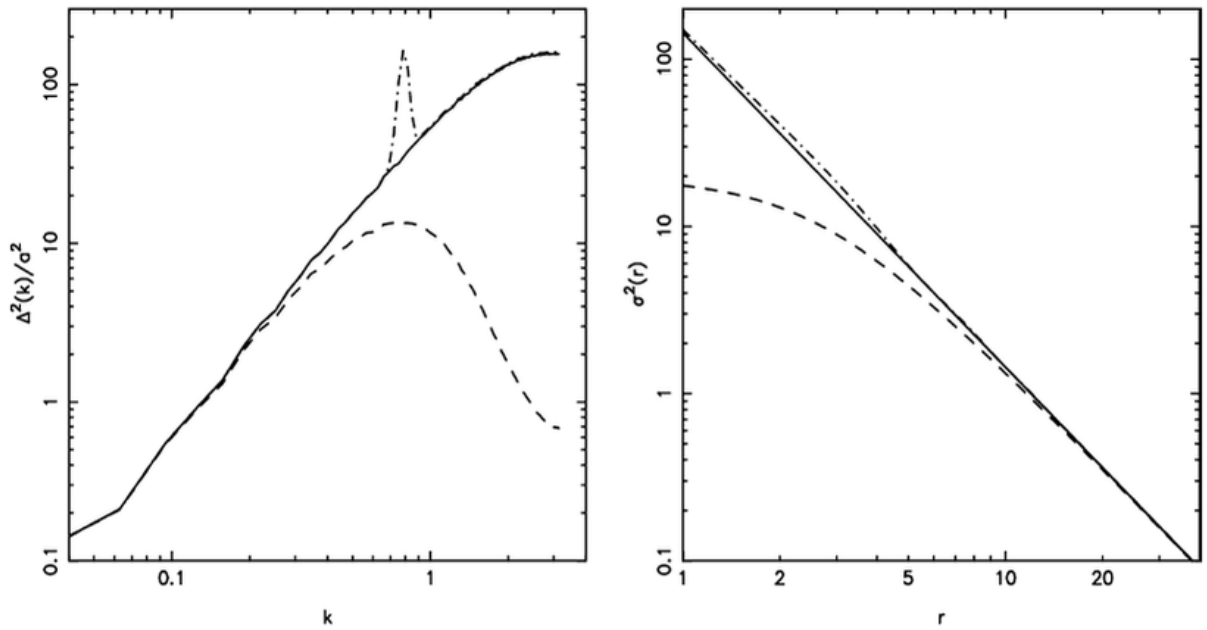

Figure 1. The left- and right-hand panels in this figure show the linearly extrapolated power spectrum $\Delta^2(k)$ and variance $\sigma^2(r)$ at the epoch $a = 1$. In both the panels, Models I, II and III are represented by the solid, dashed and dot-dashed lines, respectively.

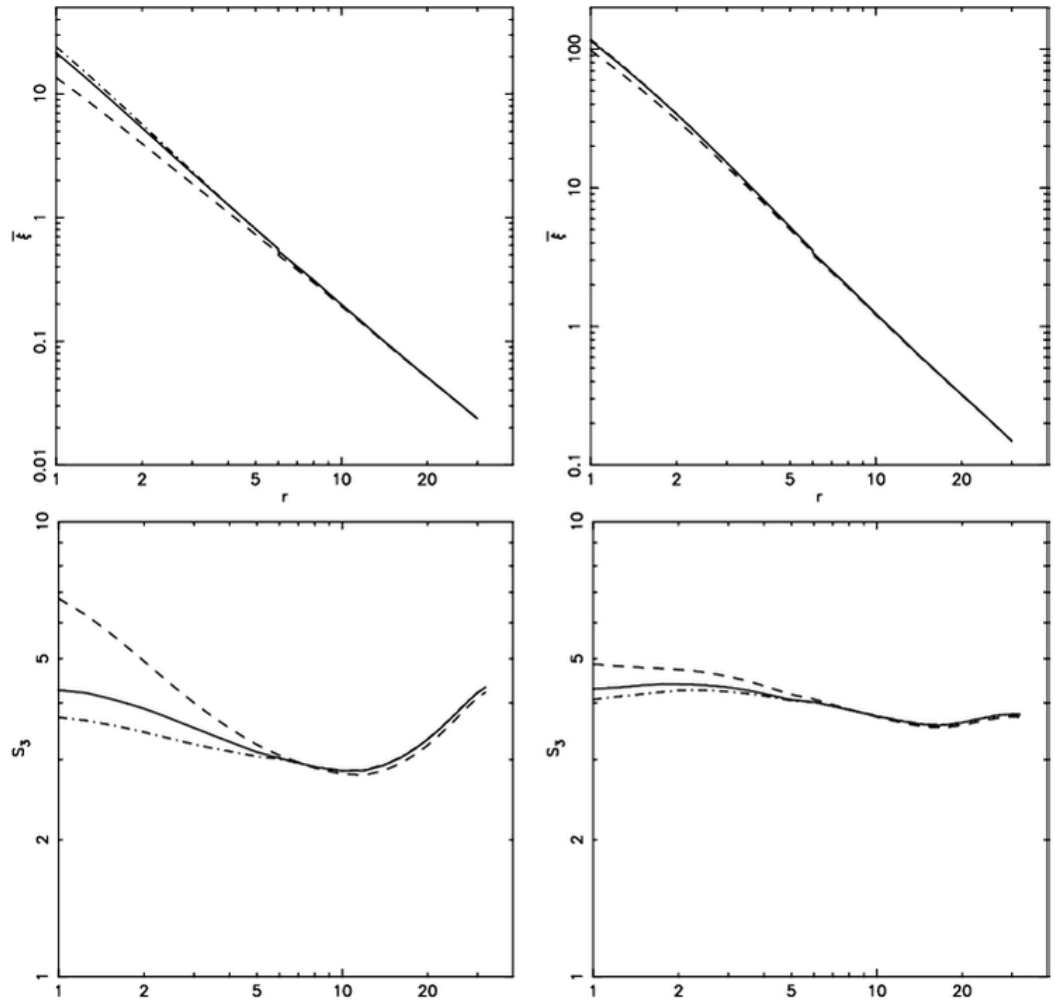
0.01
0.1
1
10
100
1
2
5
10
20
r
$\bar{\xi}$
S_3

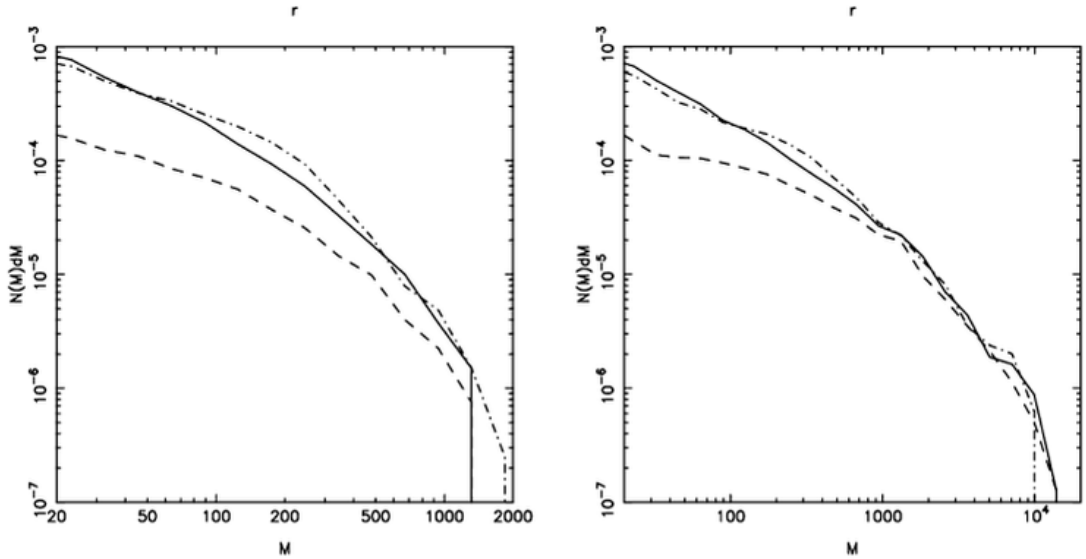

Figure 3. The first, second and third rows in this figure show the average two-point correlation function $\bar{\xi}$, skewness S_3 and comoving number density of haloes $N(M)dM$, respectively, at an early (first column) and at a later epoch (second column). Different models in all the panels are represented by the same line styles as in Fig. 1.

STUDY 2

Effects of the size of cosmological N-Body simulations on physical quantities

- Bagla, J. S., **Prasad, Jayanti** , 2006, MNRAS, 370, 993, (astro-ph/0601320), *Effects of the size of cosmological N-Body simulations on physical quantities – I: Mass Function*
- **Prasad, Jayanti** 2007, J. Astrophys.Astron. 28, 117 (astro-ph/0702557), *Effects of the size of cosmological N-Body simulations on physical quantities – II: Halo Formation and Destruction rate*
- J.S. Bagla, **Jayanti Prasad**, Nishikanta Khandai 2009, MNRAS,395,2 (arXiv:0804.1197 [astro-ph]), *Effects of the size of cosmological N-Body simulations on physical quantities - III: Skewness*

- In cosmological N-body simulations the initial power spectrum is sampled at discrete points in k space in the range $[2\pi/L_{box}, 2\pi/L_{grid}]$.
- Perturbations $k > 2\pi/L_{box}$ can be ignored since there are no significant effects or perturbations at small scales on large scale. However, that is not the case of $k < 2\pi/L_{box}$ perturbations at scales larger than the simulation volume can affect physical quantities significantly.

Our formalism

- In theory:

$$\sigma^2(r) = \int_0^\infty \frac{dk}{k}\Delta^2(k)W^2(kr)$$

$$\text{where: } \Delta^2(k) = \frac{k^3P(k)}{2\pi^2}; \quad W(kr) = 3\left(\frac{\sin kr - kr\cos kr}{k^3r^3}\right) \tag{5}$$

- In simulations:

$$\sigma^2(r, L_{box}) = \int_{2\pi/L_{box}}^{2\pi/L_{grid}} \frac{dk}{k}\Delta^2(k)W^2(kr) \approx \int_{2\pi/L_{box}}^{\infty} \frac{dk}{k}\Delta^2(k)W^2(kr)$$

$$= \int_0^\infty \frac{dk}{k}\Delta^2(k)W^2(kr) - \int_0^{2\pi/L_{box}} \frac{dk}{k}\Delta^2(k)W^2(kr)$$

$$= \sigma_0^2(r) - \sigma_1^2(r) \tag{6}$$

Results:Correction in clustering amplitude

$$\sigma_1^2(r, L_{box}) = \int_0^{2\pi/L_{box}} \frac{dk}{k} \Delta^2(k) W^2(kr)$$

$$\approx C_1 - \frac{1}{5} C_2 r^2 + \frac{3}{175} C_3 r^4 + \mathcal{O}(r^6) \quad (7)$$

where

$$C_n = \int_0^{2\pi/L_{box}} \frac{dk}{k} k^{2(n-1)} \Delta^2(k) \quad (8)$$

For power law model:$P(k) = Ak^n$

$$C_1 = \frac{A}{2\pi^2(n+3)} \left(\frac{2\pi}{L_{box}}\right)^{(n+3)} \quad (9)$$

Results:Correction in Mass function

- The Press-Schechter mass function:

$$F(M) = F_0(M) = 2\int_{\delta_c}^{\infty} \frac{1}{\sqrt{2\pi}\sigma_0(M)} \exp\left(-\frac{\delta^2}{2\sigma_0^2(M)}\right) d\delta \qquad (10)$$

- In N-body simulations we get:

$$F(M, L_{box}) = 2\int_{\delta_c}^{\infty} \frac{1}{\sqrt{2\pi}\sigma(M, L_{box})} \exp\left(-\frac{\delta^2}{2\sigma^2(M, L_{box})}\right) d\delta \qquad (11)$$

- Correction :

$$F_1(M, L_{box}) = F_0 - F = \frac{2}{\sqrt{\pi}} \int_{\frac{\delta_c}{\sigma_0(M)\sqrt{2}}}^{\frac{\delta_c}{\sigma(M,L_{box})\sqrt{2}}} \exp(-x^2)$$

$$\approx \frac{\delta_c}{\sqrt{2\pi}} \frac{\sigma_1^2}{\sigma_0^3} \exp\left(-\frac{\delta_c^2}{2\sigma_0^2}\right) \qquad (12)$$

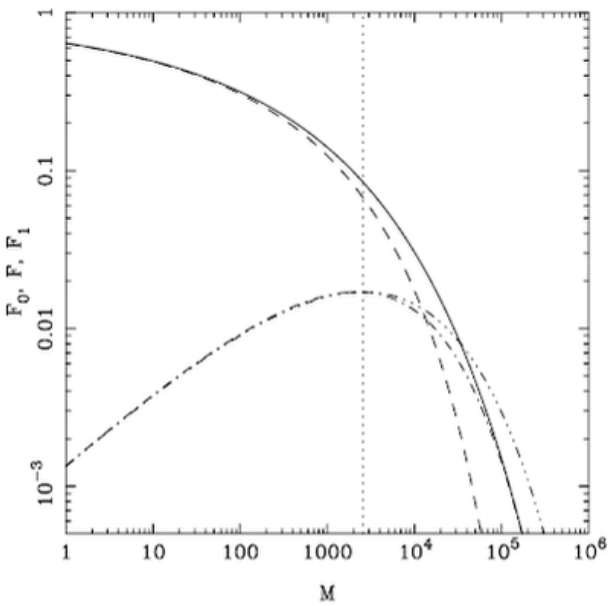

Figure 3. The Press–Schechter mass function and correction terms are plotted as a function of mass. $F_0(M)$ (solid curve), $F(M)$ (dashed curve) and $F_1(M)$ (dot–dashed curve) are shown here. The scale where $\sigma_0 = \delta_c/\sqrt{3}$ is marked with a vertical dotted line, we see that this estimate coincides with the maximum of $F_1(M)$. The correction term $F_1(M)$ is more than 10 per cent of $F_0(M)$ at this scale. Also shown is the approximate expression equation (8) for $F_1(M)$ (dot-dot-dot–dashed curve) and we note that it follows the actual curve to masses greater than M_{nl}. Mass here is plotted in units of mass of each particle and we assumed that the scale of non-linearity is 8 grid lengths.

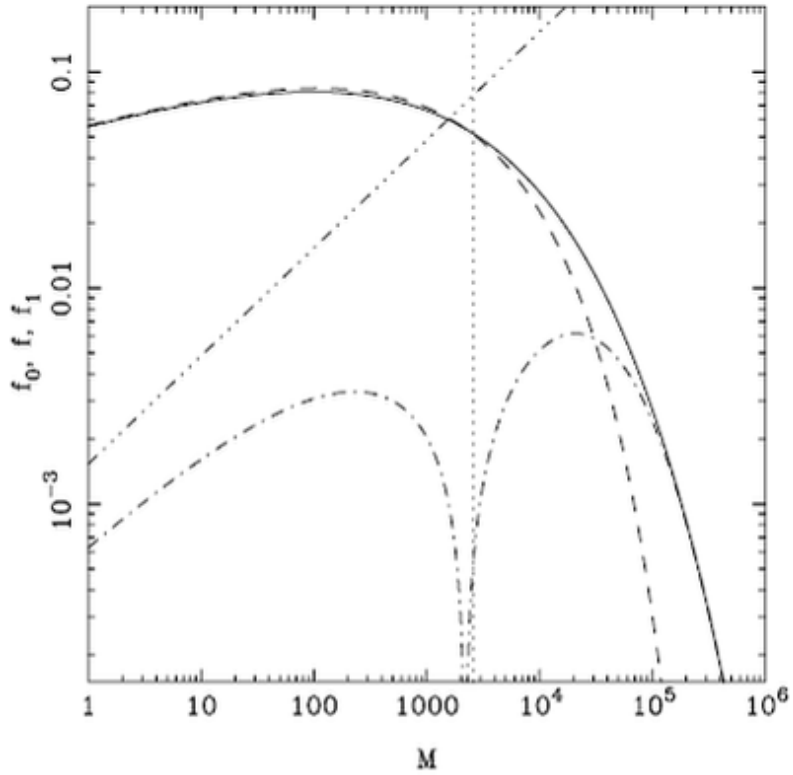

Figure 4. The Press–Schechter multiplicity function and correction terms are plotted as a function of mass. $f_0(M)$ (solid curve), $f(M)$ (dashed curve) and $f_1(M)$ (dot–dashed curve) are shown here. The scale where $\sigma_0 = \delta_c/\sqrt{3}$ is marked with a vertical dotted line, we see that this estimate coincides with change of sign for $f_1(M)$. At scales below this, the correction term $f_1(M)$ is positive and hence there are more haloes in simulation than expected in the model. Also shown is the approximate expression for $f_1(M)$ (dot-dot-dot–dashed curve). Mass here is plotted in units of mass of each particle and we assumed that the scale of non-linearity is 8 grid lengths.

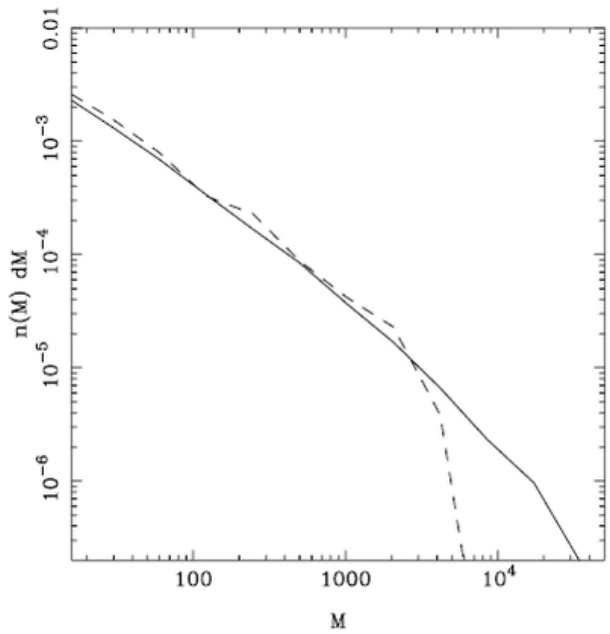

Figure 5. Shown here is the number density of haloes $n(M)\,dM$ in the mass range $M - M + \mathrm{d}M$ for these two simulations. The solid line shows the number density of haloes in the reference simulation ($L_{\mathrm{box}} = 256$). Number density of haloes in the simulation with $L_{\mathrm{box}} = 64$ Mpc is shown by the dashed line.

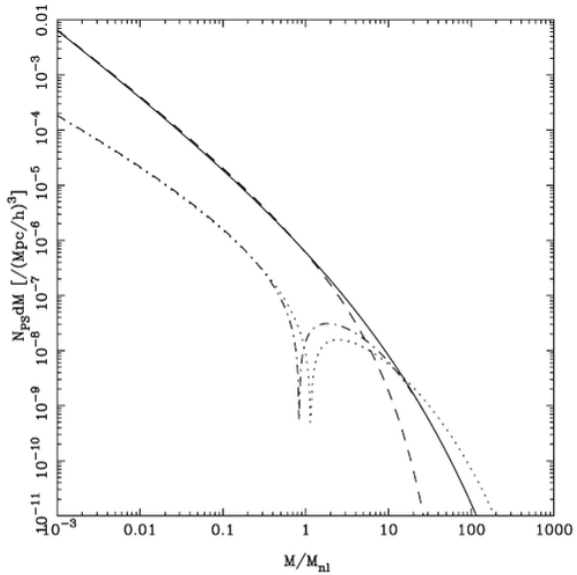

Figure 1. This figure shows the actual comoving number density $N_{PS,0}dM$ (solid line) and the comoving number density $N_{PS}\,dM$ (dashed line) which we expect in a cosmological N-body simulation at the present epoch ($z = 0$) for a power law ($n = -2$) model (see equations (9, 10)). Here we consider the size of the simulation box $128\,\mathrm{h}^{-1}$Mpc and normalize the initial power spectrum such that the scale of non-linearity (r_{nl}) at $z = 0$ is $8\,\mathrm{h}^{-1}$Mpc. In the figure, the exact (dot-dashed line) and approximate (dotted line) corrections in the comoving number density due to finite box size are also shown (see equations (11, 12)).

Table 1. This table lists characteristics of N-body simulations used in our study.

Model	Description	Cut off (k_c)
A1	Power law, $n - 2.0$	k_f
A2	Power law, $n - 2.0$	$2k_f$
A3	Power law, $n - 2.0$	$4k_f$
B1	Power law, $n - 2.5$	k_f
B2	Power law, $n - 2.5$	$2k_f$
B3	Power law, $n - 2.5$	$4k_f$
C1	ΛCDM, *WMAP*-5 BF, $L_{\rm box} = 160\,h^{-1}$ Mpc	k_f
C2	ΛCDM, *WMAP*-5 BF, $L_{\rm box} = 160\,h^{-1}$ Mpc	$2k_f$
C3	ΛCDM, *WMAP*-5 BF, $L_{\rm box} = 160\,h^{-1}$ Mpc	$4k_f$

Note. Here, the spectral index gives the slope of the initial power spectrum, and the cut-off refers to the wavenumber below which all perturbations are set to zero: $k_f = 2\pi/L_{\rm box}$ is the fundamental wave mode for the simulation box. All models were simulated using the TREEPM code (Bagla 2002; Bagla & Ray 2003; Khandai & Bagla 2008). 256^3 particles were used in each simulation, and the PM calculations were done on a 256^3 grid. Power spectra for both the A and the B series of simulations were normalized to ensure $\sigma = 1$ at the scale of 8 grid lengths at the final epoch if there is no box-size cut-off. A softening length of 0.1 grid lengths was used as the evolution of small-scale features is not of interest in this study. Simulations for both the A and the B series were done with the Einstein–deSitter background and the C series used the *WMAP*-5 best-fitting (BF) model as the cosmological background, as also for the power spectrum and transfer function.

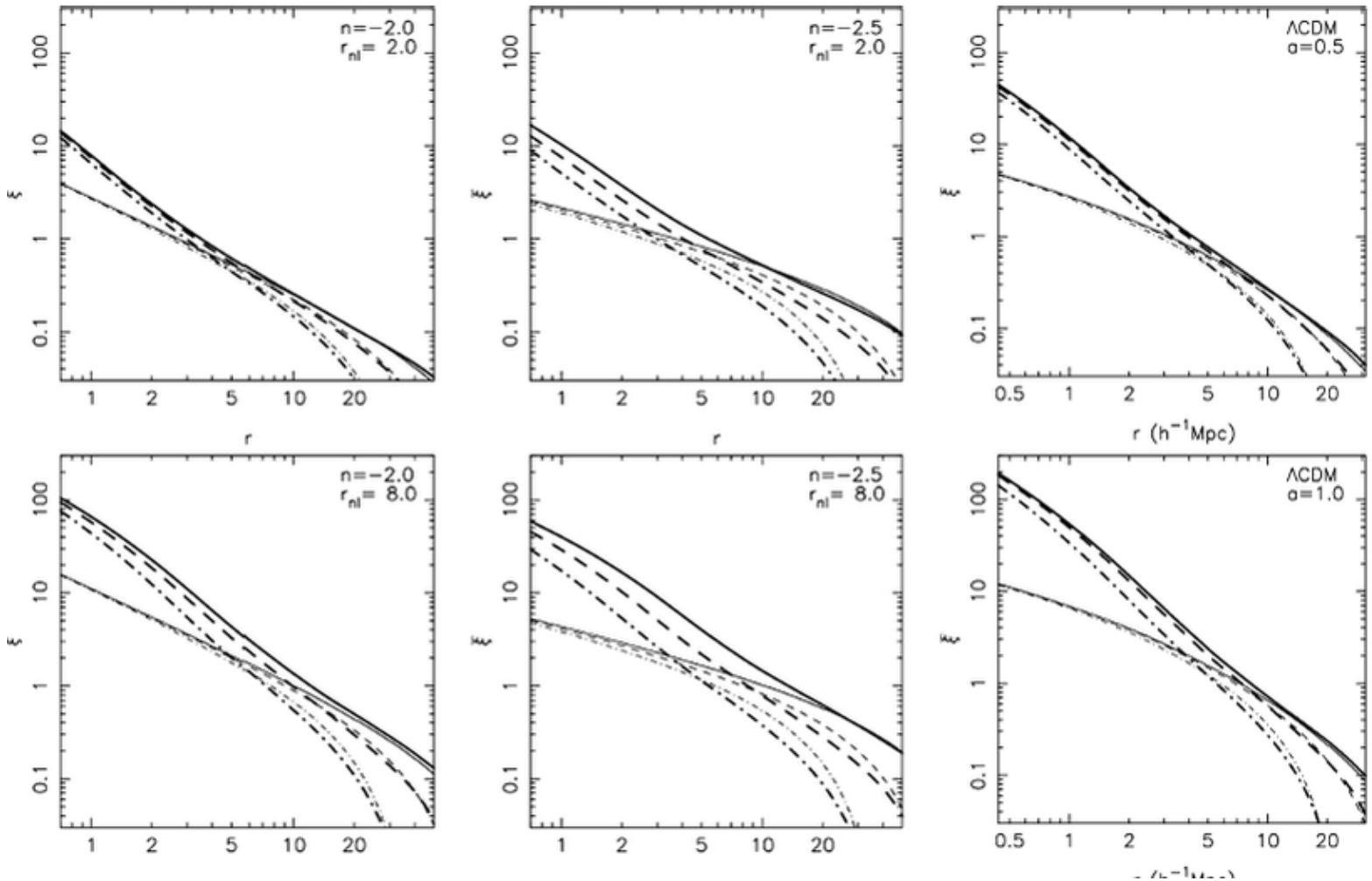
n=−2.0
r_nl= 2.0
n=−2.5
r_nl= 2.0
ΛCDM
a=0.5
n=−2.0
r_nl= 8.0
n=−2.5
r_nl= 8.0
ΛCDM
a=1.0
ξ
r
r (h^−1Mpc)
0.1
1
10
100
0.5
1
2
5
10
20

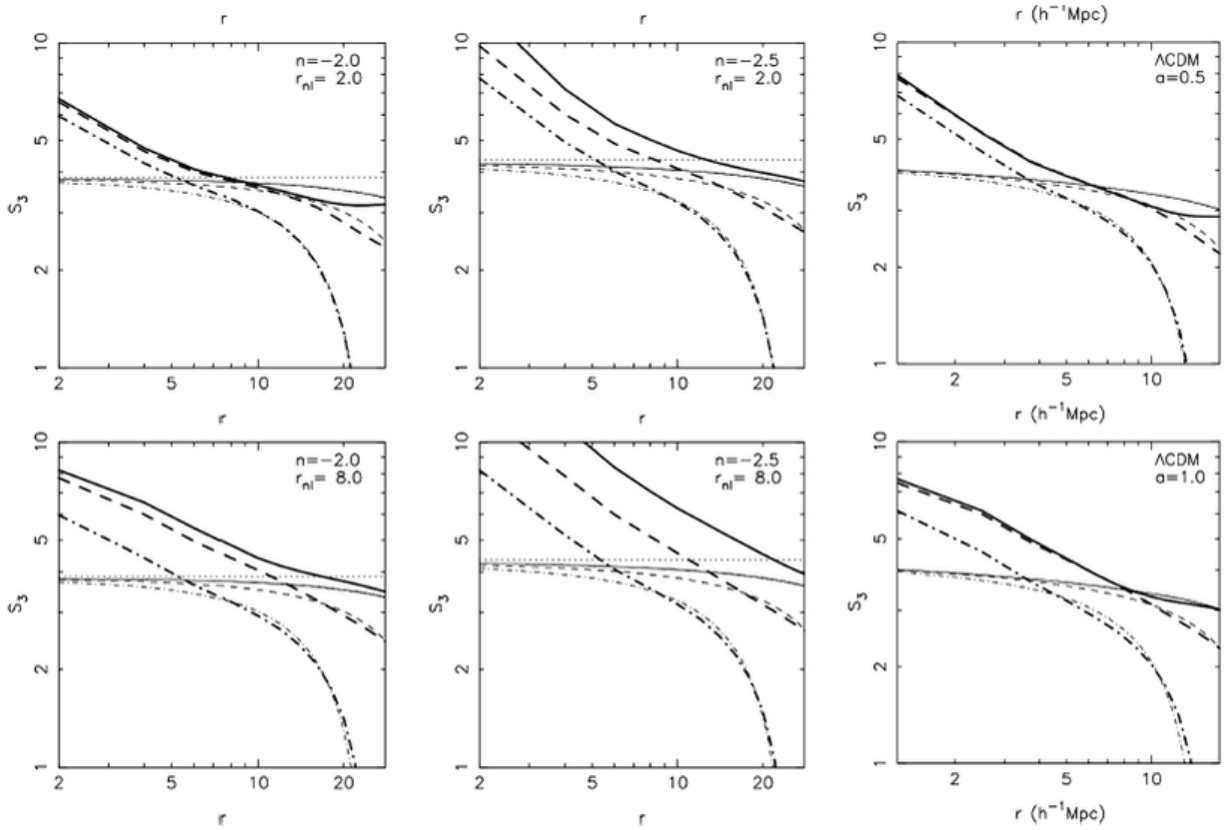

Figure 4. The first two rows in this figure show the average two-point correlation function $\bar{\xi}$, and the next two rows show skewness S_3. The first and third rows represent the early epoch, and the second and fourth rows represent the later epoch. In all the panels, models with $k_c = k_f$, $k_c = 2k_f$ and $k_c = 4k_f$ are represented by the solid, dashed and dot–dashed lines, respectively. In all the panels, corresponding to every model in simulation (thick lines) theoretical estimates (thin lines) are also shown. Horizontal dashed lines in the lower rows show the expected value of S_3 in the absence of any box-size correction for the power-law models.

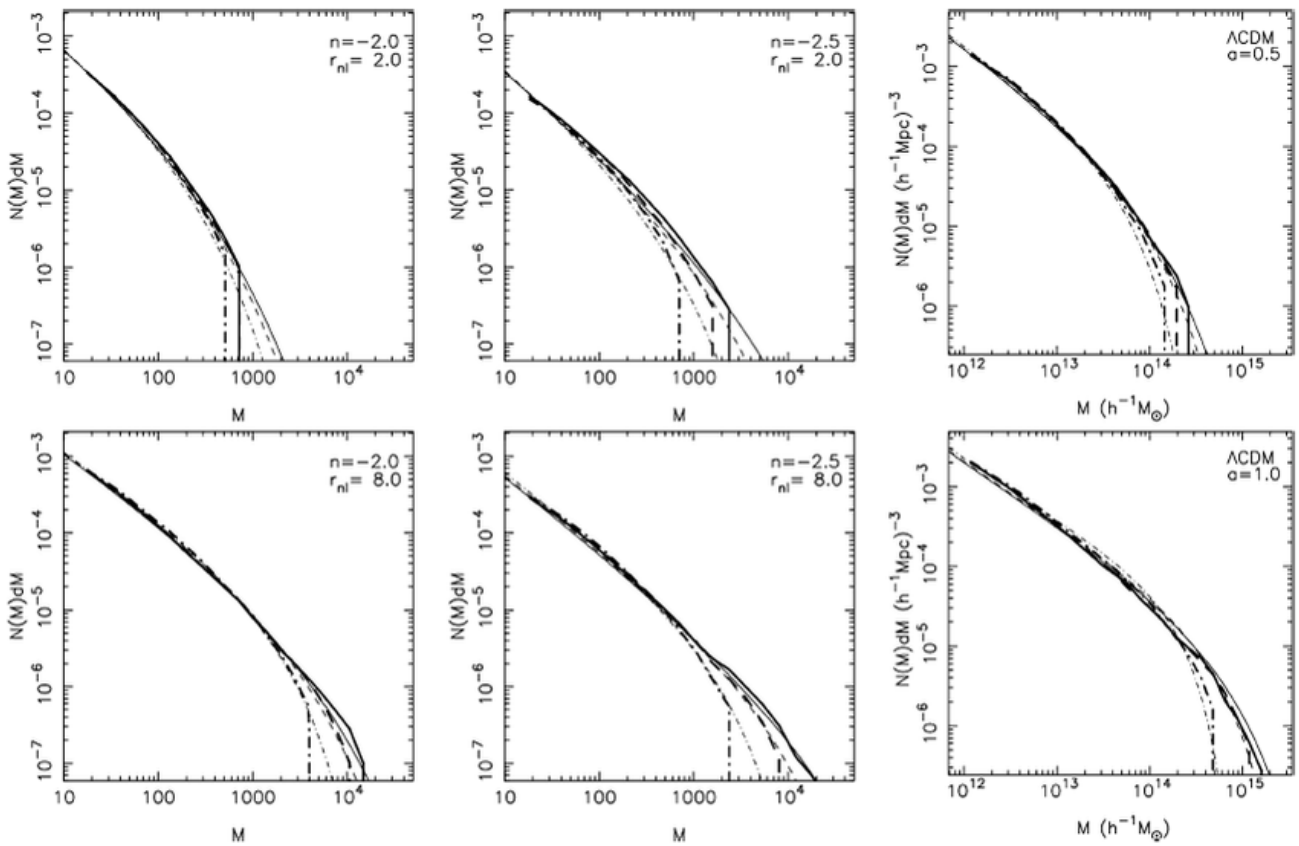

Figure 5. This figure shows the mass function $N(M)\,dM$ for the three series of simulations. The top row shows this for the early epoch and the lower row corresponds to the late epoch. In all the panels, models with $k_c = k_f$, $k_c = 2k_f$ and $k_c = 4k_f$ are represented by the solid, dashed and dot–dashed lines, respectively. In all the panels, corresponding to every model in simulation (thick lines) theoretical estimates (thin lines) are also shown.

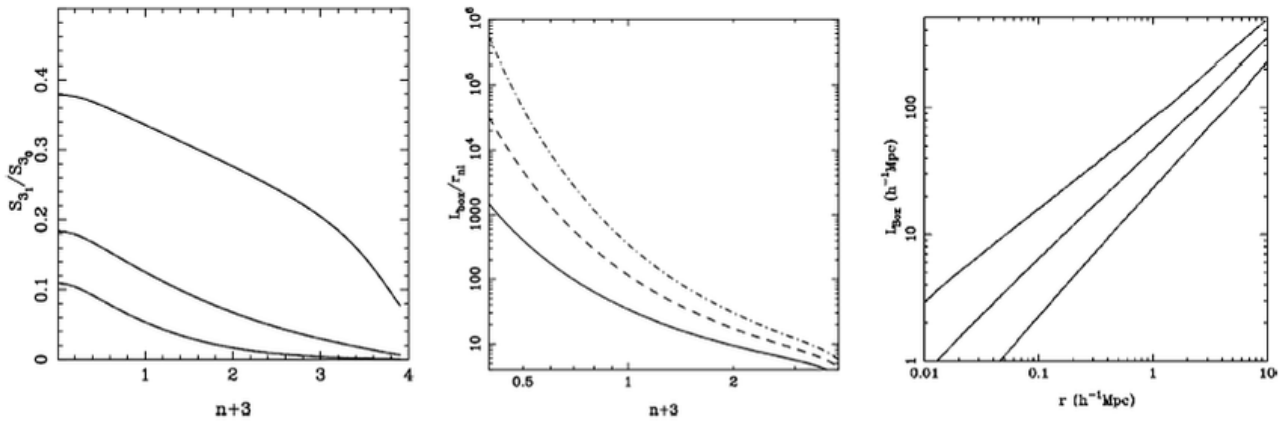

Figure 8. The left-hand panel shows the variation in the fractional correction in S_3 i.e. S_{3_1}/S_{3_0} (see equation 4), with the index of power spectrum at the scales $L_{box}/5$ (top curve), $L_{box}/10$ (middle curve) and $L_{box}/20$ (lowest line). For a given tolerance of the error in S_3 due to finite box effects, this gives us the largest scale at which the simulation may be expected to give reliable results. The middle panel shows contours of C_1 at the scale of non-linearity ($\sigma_0 = 1$) for values $C_1 = 0.01$ (top curve), 0.03 (middle curve) and 0.1 (lower curve). The contours are plotted on the $L_{box}/r_{nl} - (n+3)$ plane and indicates the box size required for reliable simulations of a given model. The right-hand panel shows contours of S_{3_1}/S_{3_0} for the ΛCDM model that best fits the *WMAP*-5 data. Contours shown are for $S_{3_1}/S_{3_0} = 0.01$, 0.03 and 0.1.

Summary & Conclusions

- In the first part of this study we have tried to understand the role played by substructure in non linear gravitational clustering.
- Since in cold dark matter models of structure formation perturbations at small scales (substructure) collapse first and lead to clustering of matter at larger scales. Therefore it becomes important to understand what role substructure can play in subsequent collapse of perturbations at larger scales.
- In cosmological N-body simulations perturbations at sub-grid scales are assumed to be zero. Our study can help to understand the effects of pre-initial condition in cosmological N-body simulations.

Summary cont...

- In the second part of our study we presented a prescription for estimating the corrections in various physical quantities of interest due to the finite size of the simulation box.
- We showed that the amplitude of clustering is underestimated at all scales when the size of the simulation volume is reduced.
- We presented explicit expressions for corrections in mass function, multiplicity function, number density and formation and destruction rate due to the finite size of the simulation box.
- We showed that the correction in mass function is maximum at scales of nonlinearity and it decreases at large as well as small scales.
- We showed that the number density of low mass haloes is overestimated and that of large mass haloes is underestimated when the size of the simulation box is reduced.

THANK YOU !